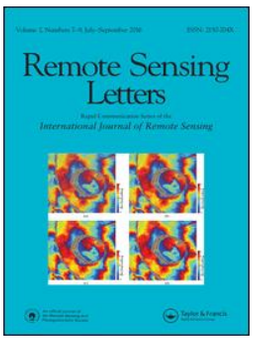

Remote Sensing Letters

ISSN: 2150-704X (Print) 2150-7058 (Online) Journal homepage: https://www.tandfonline.com/loi/trsl20

3D scattering image reconstruction based on measurement optimization of a radar network

Le Kang, Ying Luo, Qun Zhang, Xiao-Wen Liu & Bi-Shuai Liang

To cite this article: Le Kang, Ying Luo, Qun Zhang, Xiao-Wen Liu & Bi-Shuai Liang (2020) 3D scattering image reconstruction based on measurement optimization of a radar network, Remote Sensing Letters, 11:7, 697-706, DOI: 10.1080/2150704X.2020.1757781

To link to this article: https://doi.org/10.1080/2150704X.2020.1757781

Published online: 28 May 2020.

REMOTE SENSING LETTERS
2020, VOL. 11, NO. 7, 697–706
https://doi.org/10.1080/2150704X.2020.1757781

Taylor & Francis
Taylor & Francis Group

3D scattering image reconstruction based on measurement optimization of a radar network

Le Kang[a], Ying Luo[a,b], Qun Zhang[a,b], Xiao-Wen Liu[c] and Bi-Shuai Liang[a]

[a]Institute of Information and Navigation, Air Force Engineering University, Xi'an, China; [b]The Key Laboratory for Information Science of Electromagnetic Waves, Fudan University, Shanghai, China; [c]School of Information and Communications, National University of Defence Technology, Xi'an, China

ABSTRACT

For radar network, each radar can obtain the two-dimensional (2D) inverse synthetic aperture radar (ISAR) image from the corresponding observation angle independently. Taking advantage of the multi-view observation via radar network and the projection relationship in ISAR imaging, the three-dimensional (3D) image of the target can be reconstructed by the inverse-projection principle. However, it is hard to reconstruct the scattering position and coefficient simultaneously, and the network optimization should be studied to improve the reconstruction performance. To solve these problems, a novel 3D scattering image reconstruction method is proposed in this paper. Firstly, the 3D reconstruction model is built as a compressed sensing (CS) framework. Then, the network optimization for single target is transformed into the measurement matrix optimization before the 3D scattering recovery. Finally, numerical simulations under the noise scenarios and the principle prototype experiment on real data are shown to demonstrate the validity of the proposed method.

ARTICLE HISTORY
Received 14 December 2019
Accepted 13 April 2020

1. Introduction

Inverse synthetic aperture radar (ISAR) imaging is a typically surveillance technique for aerospace targets as it can generate two-dimensional (2D) electromagnetic images of the targets (Chen et al. 2016). Because a 2D ISAR image can only represent a target's scattering projection on the imaging plane determined by the flight line of the target and the line of sight (LOS) of the radar, tremendous differences in the ISAR images for the same target would be caused by differences of observation geometry. According to the ISAR imaging principle, it is difficult to extract the integrated scattering information from a 2D image. Therefore, the three-dimensional (3D) image generation is significant to obtain the whole 3D scattering distribution and structure information of aerospace targets (Liu et al. 2016). Nowadays, 3D ISAR imaging methods can mainly be categorized into three different frames including interferometric ISAR (InISAR) (Nasirian and Bastani 2014), 3D ISAR imaging (Qiu et al. 2015) and ISAR movie (Suwa, Wakayama, and Iwamoto 2011; Hui and Bai 2018).

Radar network constituted by multiple separated radars has attracted increasing attention in recent years. At first, the researches about radar network focused on the target detection

CONTACT Ying Luo luoying2002521@163.com Institute of Information and Navigation, Air Force Engineering University, Xi'an 710077, China

and tracking to provide high detection rate, 3D target tracking, optimum resource allocation of detection and tracking tasks and so on. Considering the imaging problem, a multi-target imaging task allocation method in the radar network is proposed based on the relaxed convex optimization theory (Liu et al. 2017). As the echo from different observation angles can be achieved by the radar network simultaneously, the radar network can provide additional information about the targets. Therefore, the radar network is a kind of potential system to provide the 3D images for aerospace targets different from the abovementioned frames. In our previous work, 3D image reconstruction via the radar network for spinning targets is implemented based on 0–1 programming by simulations (Liu et al. 2018, 2019). However, there are still some outstanding problems. On one hand, the reconstruction method based on 0–1 programming can only provide the position of the scatterers without the scattering coefficients. On the other hand, since the measurement of different angles is determined by the distribution of radar network, the network optimization should be studied to improve the reconstruction performance.

To solve the above problems, a novel radar network 3D scattering image reconstruction method is proposed in this paper. The main work of this paper can be mainly summarized in two points. The one is to provide the scattering position and coefficient simultaneously, and the other one is to design the radar network optimization model to improve reconstruction performance. To verify the performance of proposed method, the radar network constitutes a random distribution in the simulation part. However, an equivalent circle distribution is adopted in the experiment part as the experimental environment is limited.

2. Radar network 3D image reconstruction

2.1. Signal model

The imaging mode of radar network is shown in Figure 1. The target is supposed to fly in the far field with velocity vector v. The radar network for a target is constituted by N_r radars selected from the N_R available radars. The set of the radars in the radar network and the set of the available radars are denoted by E and E_0, respectively. The radars can obtain the ISAR images of the target independently of different observation angles. In Figure 1, (O,X,Y,Z) denotes the target Cartesian coordinate and (O,U_i,W_i) is the orthogonal plane coordinate on the imaging plane, where O is the target centre point determined by target tracking, and $i = 1, 2, \ldots, N_r$ denotes the i-th radar. The imaging plane is determined by the line of sight (LOS) and the velocity. n_i denotes the normal vector of the i-th imaging plane. In the remainder of the paper, the 3D coordinates are defined in (O,X,Y,Z) and the 2D coordinates are defined in (O,U_i,W_i).

Suppose that the transmitted signal of the i-th radar is expressed as follows

$$s_i(t_r) = p_i(t_r)\exp(\mathrm{j}2\pi f_c t_r) \tag{1}$$

where t_r is the fast time, $p_i(t_r)$ is the waveform function, and f_c is the carrier frequency. Then, the baseband echo signal can be expressed as

$$s_i(t_r) = g_i(x,y)p_i(t_r - 2R/c)\exp(-\mathrm{j}4\pi f_c R/c) + n_0 \tag{2}$$

where $g_i(x,y)$ denotes the scattering coefficient at (x,y) on the i-th imaging plane, c is the light velocity, R is the distance from the radar to the scatterers and n_0 is the noise.

To discrete the observation area with the grid width Δx and Δy, $g_i(x,y)$ can be rewritten as a scattering coefficient vector $g_i = [g]_{PQ\times 1}$, $g_{p\times Q+q} = g_i(p\Delta x, q\Delta y)$, where P and Q denote the

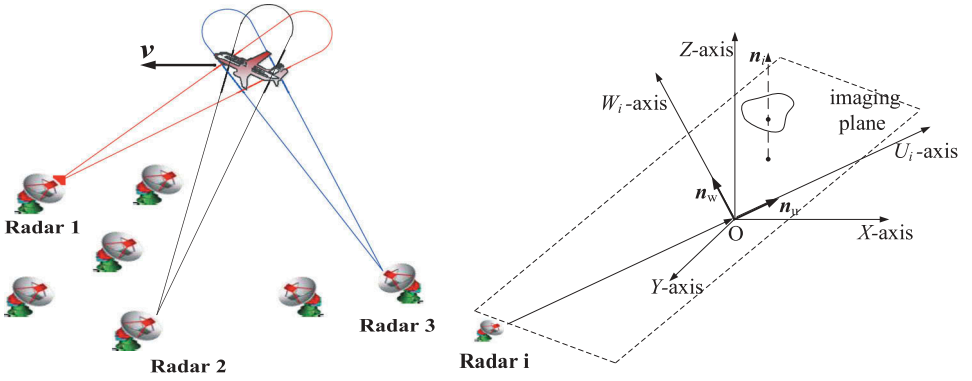

Figure 1. Radar network imaging mode. (a) The radars selected to form a network observe the target independently. (b) Geometry for radar observation.

grid number in range and azimuth, $p = 1, 2, \ldots, P, q = 1, 2, \ldots, Q$. Then, the echo signal can be rewritten as the following discrete form.

$$s_i(t_{r,n}, t_{a,m}) = \sum_{j=1}^{PQ} g_i(j) a_i(m, n, j) + n_0 \tag{3}$$

where t_a denotes the slow time, $a_i(m, n, j)$ denotes the terms in (2) except the scattering coefficient, $m = 1, 2, \ldots, M$ and $n = 1, 2, \ldots, N$ denote the range and cross-range sampling points, respectively. Furthermore, matrix form of (3) can be rewritten as

$$s_i = A_i g_i + n_0 \tag{4}$$

where $s_i = [s]_{MN\times 1}, s_{n\times M+m} = s_i(t_{r,n}, t_{a,m})$ and $A_i = [a]_{MN\times PQ}, a_{n\times M+m,j} = a_i(m, n, j)$ are the signal vector and the measurement matrix, and $n_0 = [n_{0,1}, \ldots, n_{0,MN}]^{\mathrm{T}}$ is the noise vector.

2.2. Mapping process

Suppose that point at (x_P, y_P, z_P) is projected at (x_Q, y_Q, z_Q) on the i-th imaging plane, the mapping process can be expressed as

$$[x_P \quad y_P \quad z_P]^T = \boldsymbol{D}_i (\boldsymbol{D}_i^T \boldsymbol{D}_i)^{-1} \boldsymbol{D}_i^T [x_Q \quad y_Q \quad z_Q]^T \tag{5}$$

where $\boldsymbol{D}_i = [\boldsymbol{n}_{u,i}, \boldsymbol{n}_{w,i}]$, $\boldsymbol{n}_{u,i}$ and $\boldsymbol{n}_{w,i}$ are the unit vectors along the axis U_i and W_i. Suppose $\overrightarrow{OQ} = u_Q \boldsymbol{n}_{u,i} + w_Q \boldsymbol{n}_{w,i}$, where (u_Q, w_Q) is the coordinates of the projection point in (O,U_i,W_i), the projection matrix from (O,X,Y,Z) to (O,U_i,W_i) can be written as

$$[x_P \quad y_P \quad z_P]^T = \boldsymbol{\Phi}_i [u_Q \quad w_Q]^T \tag{6}$$

where $\boldsymbol{\Phi}_i = (\boldsymbol{D}_i^T \boldsymbol{D}_i)^{-1} \boldsymbol{D}_i^T$.

We define two sets: (1) the set of scatterers on the target is denoted by C_1 and (2) the set of feasible points in the 3D space is denoted by C_2. If a point is on a normal line of an imaging plane passing through any scatterer, the point is a feasible point. Since all the scatterers are feasible points, the relationship $C_1 \subset C_2$ is obviously.

The set C_1 is defined as $C_1 = \{c_n | c_n = (\sigma_n, \overrightarrow{OS_n}), n = 1,2,...,N_s\}$, where N_s denotes the number of scatterers, σ_n and $S_n$denote the scattering coefficient and the position of the n-th scatterer in (O,X,Y,Z), respectively. To reconstruct the scattering position and coefficient simultaneously, the representation of the scatterers should be replaced by the index image. The index image of the scatterers on the target can be written as

$$X_S = [\sigma \quad S]^T \tag{7}$$

where $\sigma = [\sigma_1, ..., \sigma_{N_s}]^T$ and $S = [\overrightarrow{OS_1}, ..., \overrightarrow{OS_{N_s}}]^T$. However, if X_S is regarded as the solution, the problem will be difficult to solve because X_S is completely unknown and even the size N_s is hard to obtain.

The set C_2 is defined as $C_2 = \{b_n | b_n = (\varepsilon_n, \overrightarrow{OF_n}), n = 1,2,...,N_f\}$, where N_f is the number of feasible points, ε_n and $\overrightarrow{OF_n}$ denote the scattering coefficient and the position of the n-th feasible point in (O,X,Y,Z), respectively. The index image of the feasible points can be written as

$$\boldsymbol{X}_f = [\boldsymbol{\varepsilon} \quad \boldsymbol{F}]^T \tag{8}$$

where $\boldsymbol{\varepsilon} = [\varepsilon_1, ..., \varepsilon_{N_f}]^T$ and $\mathrm{F} = [\overrightarrow{\mathrm{OF}_1}, \overrightarrow{\mathrm{OF}_2}, ..., \overrightarrow{\mathrm{OF}_{\mathrm{N_f}}}]^{\mathrm{T}}$.

To determine the feasible points, the difference between the ISAR image and the projection is utilized. For each radar in the radar network, a point is a feasible point only when the square sum of the difference image is less than that of the ISAR image. Moreover, the union of the feasible points obtained by all radars in the network is the entire set of the feasible points. By ensuring the feasible points, the size N_f and the position set $\mathbf{F}$ in $\mathbf{X}_f$ are known. As $\mathbf{X}_f$ is a sparse matrix with a fixed size, it is a suitable solution to be reconstructed. Then, the mapping process for the i-th radar in the radar network can be expressed as

$$\mathbf{F_i}(\mathbf{X_f}) = \mathbf{\Psi_i X_f}, \mathbf{\Psi_i} = \begin{bmatrix} 1 & \\ & \mathbf{\Phi}_i \end{bmatrix} \tag{9}$$

where $\mathbf{\Phi}_i = (\mathbf{D}_i^T \mathbf{D}_i)^{-1} \mathbf{D}_i^T$ is the projection matrix of the i-th radar.

2.3. Network optimization

There are two issues should be minimized to establish the reconstruction model based on compressed sensing (CS): (1) the number of the scatterers, and (2) the reconstruction error. To measure the reconstruction error, the sum of the differences between all the projection images and the ISAR images should be calculated. Then, the i-th ISAR image g_i should be rewritten as $\mathbf{I}_i = [\boldsymbol{g}'_i \quad \mathbf{\Phi}_i \mathbf{F}]^T$, where $\boldsymbol{g}'$ is the rearrangement of $\boldsymbol{g}'$ according to the order of $\mathbf{\Phi}_i \mathbf{F}$. Then the reconstruction error can be expressed as

$$\sum_{i=1}^{N_r} \|\mathbf{\Psi_i X_f} - \mathbf{I_i}\|_2^2 = \|\mathbf{HX} - \mathbf{\Gamma}\|_2^2 \tag{10}$$

where $\|\cdot\|_2$ is the 2-norm operator,$H = [\mathbf{\Psi_1}, \mathbf{\Psi_2}, ..., \mathbf{\Psi_{N_r}}]$,$\Gamma = \mathrm{diag}(\mathbf{I}_1, \mathbf{I}_2, ..., \mathbf{I}_{N_r})$ and $X = \mathrm{diag}(X_f, X_f, ..., X_f)$. Then, the CS model to reconstruct the 3D scattering can be established as

$$\min \|\mathbf{X}\|_0 \mathrm{s.t.} \quad \|\mathbf{HX} - \mathbf{\Gamma}\|_2^2 < \eta_0 \tag{11}$$

where $\|\mathbf{X}\|_0$ denotes the sparsity of the scatterers on the target and η_0 is a small threshold related to environmental noise.

As the CS model of 3D scattering reconstruction is established, the distribution optimization of radar network can be regarded as the measurement matrix optimization. In the CS framework, a widely used criteria to evaluate the measurement matrix $\mathbf{H}$ is the worst-case mutual coherence $\mu(\mathbf{H})$, which is defined as the maximum of the mutual coherence matrix $\mathbf{H^T H}$ except the diagonal elements. The mutual coherence operator of matrix is defined as $U(\cdot)$. Then, $U(H)$ can be expressed as

$$\mathbf{U}(\mathbf{H}) = \begin{bmatrix} \mathbf{U}(\mathbf{\Phi_1}) & \mathbf{U}(\mathbf{\Phi_1}, \mathbf{\Phi_2}) & \cdots & \mathbf{U}(\mathbf{\Phi_1}, \mathbf{\Phi_{N_r}}) \\ \mathbf{U}(\mathbf{\Phi_2}, \mathbf{\Phi_1}) & \mathbf{U}(\mathbf{\Phi_2}) & \cdots & \mathbf{U}(\mathbf{\Phi_2}, \mathbf{\Phi_{N_r}}) \\ \cdots & \cdots & \ddots & \cdots \\ \mathbf{U}(\mathbf{\Phi_{N_r}}, \mathbf{\Phi_1}) & \mathbf{U}(\mathbf{\Phi_{N_r}}, \mathbf{\Phi_2}) & \cdots & \mathbf{U}(\mathbf{\Phi_{N_r}}) \end{bmatrix} \tag{12}$$

Thus, the worst-case mutual coherence of H can be expressed as

$$\mu(\mathbf{H}) = \max\{\mathbf{U}(\mathbf{\Phi_i}, \mathbf{\Phi_j}), \mathbf{1} \le \mathbf{i}, \mathbf{j} \le \mathbf{N_r}, \mathbf{i} \neq \mathbf{j}\} \tag{13}$$

which means that the reconstruction performance can be judged by the maximum mutual coherence between each two projection matrixes of the radars. Many previous studies have investigated that small worst-case mutual coherence can produce high probabilistic guarantees for good reconstruction performance. So the radar network optimization model can be expressed as

$$\min_{E} \left\{ \max_{1 \le i,j \le N_r, i \neq j} \mathbf{U}(\mathbf{\Phi_i}, \mathbf{\Phi_j}) \right\} \text{s.t.} E \subset E_0 \tag{14}$$

where E and E_0 are the set of the radars in the radar network and the set of the available radars, respectively. Since the U_i-axis is perpendicular to the axis W_i-axis, $\boldsymbol{n_{u,i}} \cdot \boldsymbol{n}_{w,i} = 0$, $\boldsymbol{n}_{u,i} \cdot \boldsymbol{n}_{\mathrm{u},i} = 1$and $\mathbf{\Phi}_i = [\boldsymbol{n}_{u,i}, \boldsymbol{n}_{w,i}]^T$ are satisfied. As the projection matrix $\mathbf{\Phi}_i$ is determined by $n_{u,i}$ and $n_{w,i}$ of the imaging plane, $U(\mathbf{\Phi}_i, \mathbf{\Phi}_j)$ is determined by the angle between the imaging planes of the i-th radar and j-th radar.

2.4. Reconstruction algorithm

The proposed algorithm is depicted in Algorithm 1, where E and E_0 are the set of the radars in the radar network and the set of the available radars, |E| is the number of elements in E, e_i and e_j are the i-th and j-th elements in the set E, N_x, N_y and N_z, are the number of grids along X-axis, Y-axis and Z-axis, β_i is the feasible point set of the i-th radar and α is the entire set of the feasible points. The process of the presented reconstruction algorithm is divided into four steps. The first step is network optimization. The radar network is initialized to contain all the radars. Then, $\mathbf{U}(\mathbf{H})$ is calculated and the diagonal elements are set to zero. The maximum element of $\mathbf{U}(\mathbf{H})$ is removed and the radar network E is updated till |E| is no more than N_r. The second step is generation of 2D ISAR images, in which the range-doppler (RD) algorithm is utilized. The third step is to ensure the feasible spatial point set. For the i-th radar, any point belongs to the feasible point set $\beta_i$only if $||\mathrm{F}_i(\mathbf{X}) - \mathbf{I}_i||_2^2 < ||\mathbf{I}_i||_2^2$. Moreover, the union of all the sets β_i is the entire set of the feasible points α. The final step is to solve (11) by CS algorithm. We chose the orthogonal matching pursuit (OMP) algorithm considering the computational efficiency.

Algorithm 1

Input: Coordinates of the available radars; Velocity v of the target; Position O of the target center; The radar number N_r of the subnet.

Step 1) Network Optimization:
Initialize the set $E = E_0$; Calculate $\mathbf{U}(\mathbf{H})$ and set the diagonal elements to zero;
while $|E| > N_r$
Find the maximum element $\mu_{i,j}$ in $\mathbf{U}(\mathbf{H})$; Update $E = E - \{e_i, e_j\}, \mu_{i,j} = 0$;
end
Step 2) Obtain the 2D ISAR imaging results $\{\mathbf{I}_1, \mathbf{I}_2, \ldots, \mathbf{I}_{N_r}\}$ by RD algorithm.
Step 3) Ensure the set of feasible spatial points
for $i = 1 : N_r$
  Set $\sigma = 0$ and $\beta_i = \emptyset$;
    for $k = 1 : N_x N_y N_z$
      Set $\sigma_k = 1$; **if** $||\mathrm{F}_i(\mathbf{X}) - \mathbf{I}_i||_2^2 < ||\mathbf{I}_i||_2^2$, update $\beta_i = \beta_i \cup k$;
    end for
  Update $\alpha = \alpha \cup \beta_i$
end for
Step 4). Solve the 3-D reconstruction model by OMP algorithm
Output: 3D scattering matrix X

3. Experiments

3.1. Simulation results

Since the proposed method is not limited by the radar network distribution, the random distributed radar network is adopted in the simulation part. As shown in Figure 2, 20 available radars are randomly distributed in the space. The target scattering coefficients are randomly generated. The velocity is (−50, −500, −20) m s^{-1}, $N_r = 3$. The origin of coordinates is set to the initial position of the target centre. According to the proposed network optimization method, three radars located at (9.5, −5.5, −31.5) km, (−4, −18.5, −32.7) km and (22, −19, −32.1) km are selected to form the subnet, as shown in Figure 2. For the transmitted linear-frequency-modulated signals, the pulse duration is 1us, the carrier frequency is 5 GHz, the bandwidth is 300 MHz and the pulse repetition frequency is 1000 Hz. Since the range resolution and cross-range resolution are 0.3 m, the grid interval of the 3D space is 0.25 m. As shown in Figure 3, the 2D ISAR images of Radar 1 to Radar 3 are obtained by RD algorithm, and the 3D scattering reconstruction result is provided. To evaluate the optimization performance, 500 different radar network distributions are randomly generated for different signal-noise ratio (SNR). Then, the variation of the root-mean-square error (RMSE) with SNR is shown in Figure 4. The position error of the optimized subnet is less than that of the random subnet. When SNR is over −15 dB, the RMSE of position is less than 0.1 m, which can be accepted as the resolution

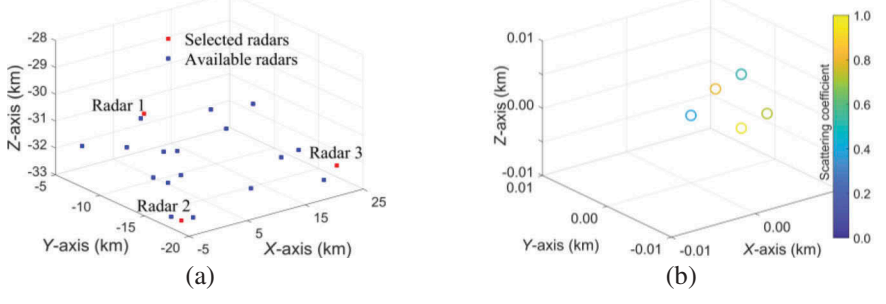

Figure 2. Radar network distribution and target model. (a) Available radar layouts and the selected radars. (b) Target model.

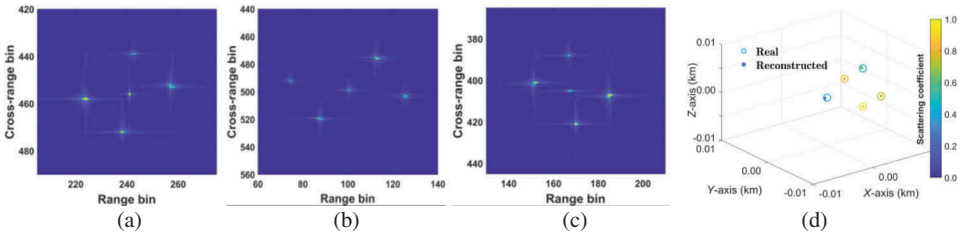

Figure 3. Simulation results of the target model consisted of 5 ideal point scatterers when SNR is 5 dB. (a), (b) and (c) are the 2D ISAR images obtained by Radar 1, Radar 2 and Radar 3, respectively. In (d), the real positions and the reconstructed results are denoted by the coloured circles and the coloured solid circles, respectively.

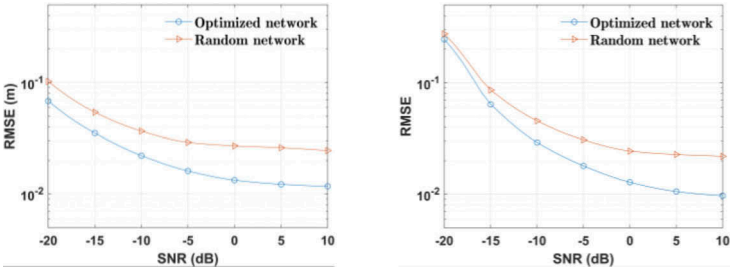

Figure 4. Variation of the RMSE with SNR. (a) Reconstruction error of position. (b) Reconstruction error of scattering coefficient.

of ISAR images is 0.3 m. For the certain distribution formed by 5 radars at (−2, −6, −30) km, (0, −12, −32) km, (0, −17, −30) km, (25, −10, −33) km and (15, −20, −32) km, the remonstration results are generated by all the possible subnets when SNR is 5 dB. Table 1 shows the RMSE of different subnets. The RMSE of the optimized subnet (2, 4, 5) in Table 1 is the smallest.

3.2. Experiment results

The experiment system is shown in Figure 5. In the experiment part, an equivalent circle distribution for the radar network is adopted as the experimental environment is limited. The target is constituted by five metal balls and it can rotate around the vertical axis. Since the target can be observed at several rotation angles, it is equal to the observation from a radar network with circle distribution. The initial coordinates of the metal balls are (0, 0, 50) cm, (18, 18, 0) cm, (18, −18, 0) cm, (−18, 18, 0) cm and (−18, −18, 0) cm. For the transmitted linear frequency modulated continuous wave, the carrier frequency is 14 GHz, the bandwidth is 6 GHz and the pulse duration is 4 ms. In each observation angle, the azimuth synthetic angle is 14.4° and the cross-range sampling number is 400. The range resolution and cross-range resolution are 2.5 cm and 4.2 cm, respectively.

Table 1. RMSE of the reconstruction results.

Subnet	Position (m)	Coefficient	Subnet	Position (m)	Coefficient
1,2,3	0.6809	0.2751	1,4,5	0.0684	0.0589
1,2,4	0.1763	0.0906	2,3,4	0.2653	0.2302
1,2,5	0.3283	0.2439	2,3,5	0.2904	0.1827
1,3,4	0.1206	0.0730	2,4,5	0.0462	0.0326
1,3,5	0.1846	0.1078	3,4,5	0.2175	0.1518

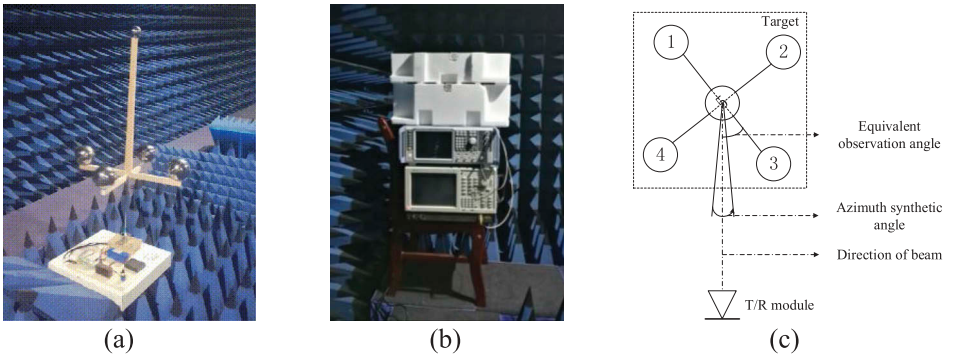

Figure 5. The experiment system. (a) The target. (b) The measurement set-up. (c) The diagram of from top view.

The 2D ISAR imaging results observed from 30°, 150°, 270°, 47°, 132° and 198° are shown in Figure 6 (a–f), respectively. The first three equivalent observation angles are provided by the proposed network optimization method and the last three equivalent observation angles are randomly generated. The comparison of 3D reconstruction results of the optimized angles and the random angles is shown in Figure 7.

We choose one fixed angle as 0°, and the other two angles are set from 10° to 350° with interval of 10°. Then, all the possible distributions are traversed. To evaluate the reconstruction performance, the weighted root-mean-squared error (WRMSE) defined by $\Lambda = (\sum_{n=1}^{N_s} \sigma_n |d_n|^2)^{1/2}$ is used, where Δd_n denotes the position error of the n-th scattering centres. For each distribution, the 3D remonstration result is generated and the WRMSE is calculated. Figure 8 shows the WRMSE for all the distributions. The WRMSE is 2.296 cm as the distribution is (0°, 120°, 240°), which is the smallest WRMSE in all the distributions. The experiment results show that the optimized angles perform better reconstruction performance than the random angles.

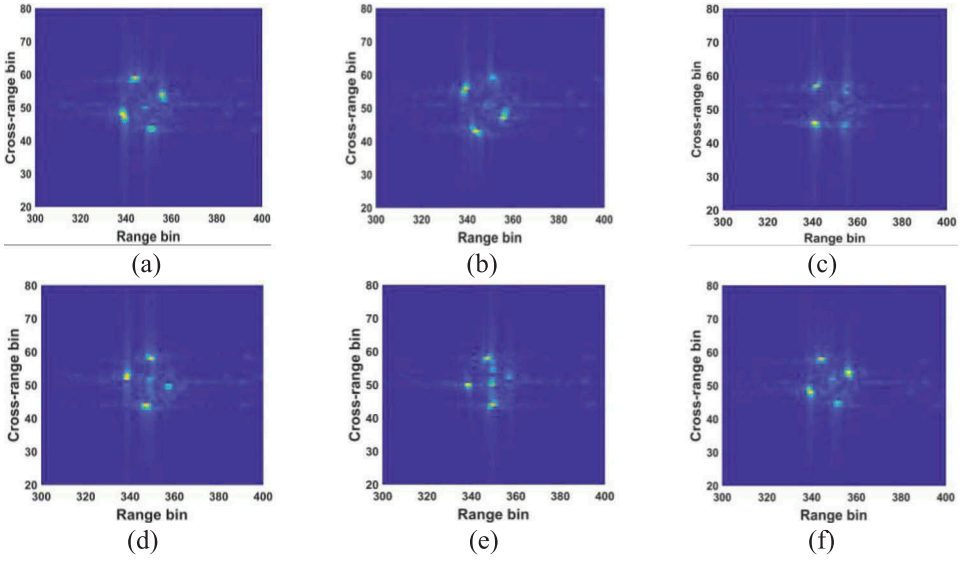

Figure 6. 2D ISAR imaging results of the five balls from different angles. (a) to (f) are observed from 30°, 150°, 270°, 47°, 132° and 198°, respectively.

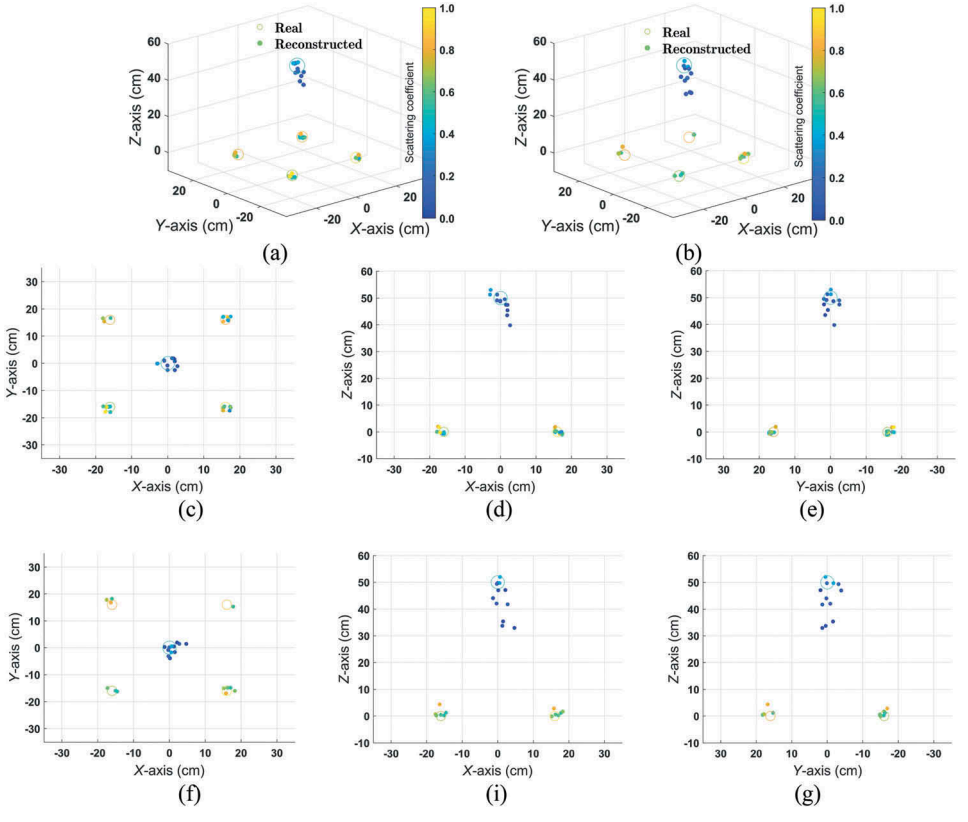

Figure 7. Comparison of 3D reconstruction results of the optimized angles and the random angles. (a) 3D reconstruction results of the optimized angles. (b) 3D reconstruction results of the random angles. (c), (d) and (e) are the three views of (a). (f), (i) and (g) are the three views of (b).

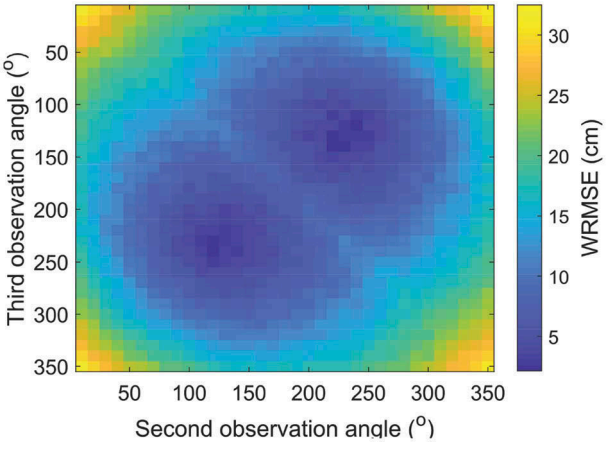

Figure 8. The WRMSE for all the distributions as the first observation angle is 0°.

4. Conclusions

In this letter, the network optimization in radar network 3D scattering reconstruction is solved in the CS framework. The main work of this paper can be mainly summarized in two points. The first one is to build a CS model to reconstruct the scattering position and coefficient simultaneously, and the other one is to design the radar network optimization model to improve reconstruction performance. Finally, the numerical simulations and the principle prototype experiment in the microwave anechoic chamber are shown to demonstrate the validity of the proposed method.

Acknowledgments

The authors would also like to thank the Associate Editor and the anonymous reviewers for their helpful comments and suggestions.

Funding

This work was supported in part by the National Natural Science Foundation of China under [Grant 61631019, 61801516 and 61971434] and the Natural Science Basic Research Program of Shannxi Province under [Grant 2019JQ-238].

References

Chen, Y. J., Q. Zhang, Y. Luo, and Y. A. Chen. 2016. "Measurement Matrix Optimization for ISAR Sparse Imaging Based on Genetic Algorithm." *IEEE Geoscience and Remote Sensing Letters* 13 (12): 1875–1879. doi:10.1109/LGRS.2016.2616352.

Hui, Y., and X. R. Bai. 2018. "RID Image Series-based High-resolution Three-dimensional Imaging of Micromotion Targets." *Journal of Radars* 7 (5): 548–556.

Liu, L., F. Zhou, X. R. Bai, M. L. Tao, and Z. J. Zhang. 2016. "Joint Cross-Range Scaling and 3D Geometry Reconstruction of ISAR Targets Based on Factorization Method." *IEEE Transaction on Image Processing* 25 (4): 1740–1750. doi:10.1109/TIP.2016.2526905.

Liu, X. W., Q. Zhang, Y. C. Chen, L. H. Su, and Y. J. Chen. 2017. "Task Allocation Optimization for Multi-Target ISAR Imaging in Radar Network." *IEEE Sensors Journal* 18 (1): 122–132. doi:10.1109/JSEN.2017.2771804.

Liu, X. W., Q. Zhang, L. Jiang, J. Liang, and Y. J. Chen. 2018. "Reconstruction of Three-Dimensional Images Based on Estimation of Spinning Target Parameters in Radar Network." *Remote Sensing* 12 (10): 1997–2022. doi:10.3390/rs10121997.

Liu, X. W., Q. Zhang, S. Q. Liu, Y. C. Chen, and L. Sun. 2019. "A 3D Image Reconstruction Technique for Spinning Targets Based on Radar Networks." *Remote Sensing Letters* 10 (2): 158–167. doi:10.1080/2150704X.2018.1532127.

Nasirian, M., and M. H. Bastani. 2014. "A Novel Model for Three-Dimensional Imaging Using Interferometric ISAR in Any Curved Target Flight Path." *IEEE Transaction on Geoscience and Remote Sensing* 52 (6): 3236–3245. doi:10.1109/TGRS.2013.2271875.

Qiu, W., M. Martorella, J. X. Zhou, H. Z. Zhao, and Q. Fu. 2015. "Three-dimensional Inverse Synthetic Aperture Radar Imaging Based on Compressive Sensing." *IET Radar Sonar Navigation* 9 (4): 411–420. doi:10.1049/iet-rsn.2014.0260.

Suwa, K., T. Wakayama, and M. Iwamoto. 2011. "Three-Dimensional Target Geometry and Target Motion Estimation Method Using Multistatic ISAR Movies and Its Performance." *IEEE Transaction on Geoscience and Remote Sensing* 49 (6): 2361–2373. doi:10.1109/TGRS.2010.2095423.

Yan, J. K., H. W. Liu, W. Q. Pu, H. L. Liu, Z. Liu, and Z. Bao. 2017. "Joint Threshold Adjustment and Power Allocation for Cognitive Target Tracking in Asynchronous Radar Network." *IEEE Transaction on Signal Processing* 65 (12): 3094–3106. doi:10.1109/TSP.2017.2679693.